DESIGN AND CONTROL OF A FAULT-TOLERANT ACTIVE MAGNETIC BEARING SYSTEM FOR AIRCRAFT ENGINES

James P. Lyons, Mark A. Preston, Ram Gurumoorthy, and Paul M. Szczesny
General Electric Corporate Research and Development
Schenectady, New York, USA

ABSTRACT

This paper presents a fault-tolerant rotor suspension system targeted at aircraft engine applications or other high reliability applications. Fault-tolerant electromagnetic actuators along with associated controls have been designed, constructed, and tested. An innovative 3 axis radial bearing structure is presented along with control algorithms for redundant force control and rotor position measurement.

INTRODUCTION

Active magnetic bearings provide revolutionary advantages over conventional bearing systems for applications such as gas turbine aircraft engine rotor support including improved vibration/stability characteristics and greatly extended bearing service life. The marriage of active magnetic bearings with innovative structural design and advanced materials will enable major performance increases in future gas turbine engines. To achieve these performance advantages, however, the reliability and fault-tolerance aspects of the rotor suspension system must be addressed.

The active magnetic bearing system developed has 8 control axes available to provide the 5 axes of control required for rotor suspension, thus supplying 3 on-line redundant control axes. Innovative electromagnetic actuator structures have been developed for both axial and radial magnetic bearings. Each radial bearing has 3 magnetically isolated control axes, any 2 of which are sufficient to maintain control of rotor position.

The redundant magnetic bearing structures are designed to be powered from a fault-tolerant engine electrical system as illustrated by the advanced aircraft engine electric system of Figure 1. This conceptual system relies on 3 independent 270 vdc buses for distribution amongst a variety of loads. The electric distribution system is designed for 50% over-capacity i.e. each bus designed for 50% of the needed system capacity, thereby requiring 2 of the 3 buses at any time in order to avoid system failure.

The 3 radial magnetic bearing control axes are angularly separated by 60 degrees, thereby producing an inherent coupling between the axes. It is not possible to independently control each axis as in an orthogonal radial bearing structure and each radial bearing must be controlled as a coupled structure. The control algorithms must transform signals to and from the coupled 3 axis reference frame of the physical structure to an orthogonal 2 axis virtual reference frame. These transformations are subject to individual axis availability and are capable of accommodating axis failures.

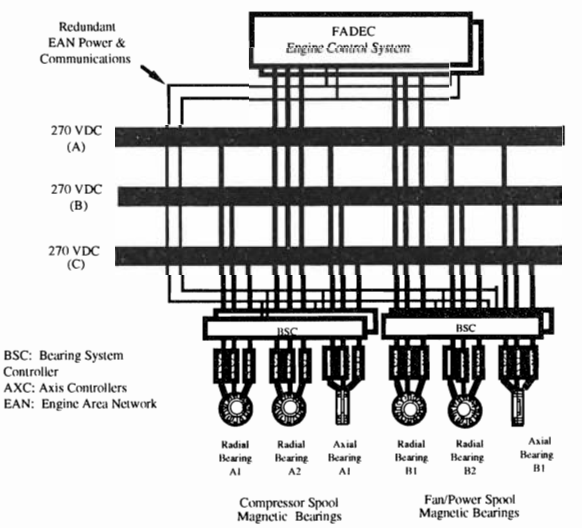

Figure 1: More Electric Engine Electrical System

A DSP based controller has been developed to implement the requisite control algorithms. The DSP

controller partitions the rotor suspension control into 2 hierarchical levels. The lowest level is an *axis controller* which provides a smart self-protecting force actuator for each control axis. The second level is the *bearing system controller* which provides for control of the rotor position, along with vibration and unbalance control.
The physical design of a high speed laboratory test rig, capable of rotating at 25,000 rpm, is also presented. The test rig has been designed to simulate the dynamics of a small gas turbine aircraft engine, incorporating bending-mode and critical-speed traversals. This test rig has been used for proof of principle demonstrations of these fault-tolerant concepts.

ELECTROMAGNETIC ACTUATORS

Figure 2 shows a fault-tolerant radial magnetic bearing with 3 radial control axes which are made up of 12 electromagnetic stator poles organized into 6 force-producing pole-pairs with 60° radial spacing. Two pole-pairs at 180° radial separation combine to create a single control axis. The 3 control axes (Figure 3) cooperate to control the rotor position by controlling the net forces along the virtual y and z axes.

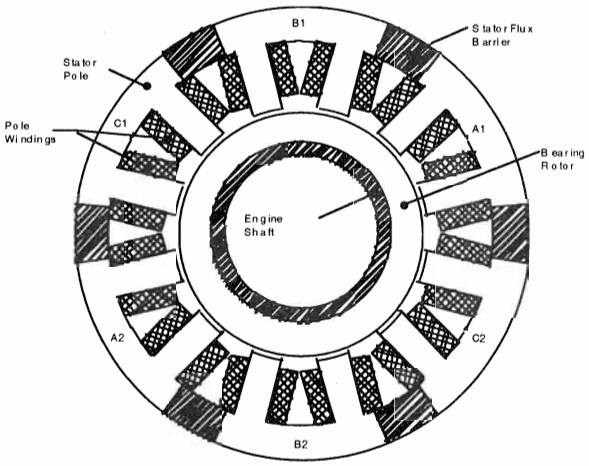

Figure 2: Fault-Tolerant Radial Magnetic Bearing

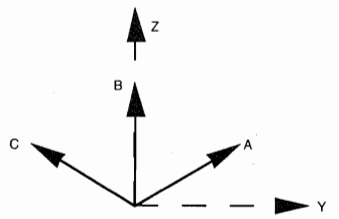

Figure 3: Radial Bearing Control Axes

The stator core is segmented with non-magnetic sections in order to minimize the magnetic coupling between adjacent pole-pairs. Figure 4 is a finite-element flux plot - each line represents 1% of flux - showing about 2% magnetic coupling to each adjacent axis. The magnetic isolation provided by the stator segmentation allows non-faulted force-actuation pole-pairs to continue functioning in the proximity of faulted magnetic poles. Since any 2 of the 3 (or more) control axes are sufficient to maintain rotor suspension, the third control axis in this magnetic structure provides inherent redundancy and given appropriate control measures, continued bearing operation in the presence of a variety of faults (e.g. faulted magnetic poles, power electronic shorts, phase power loss, etc.) is possible. Greater inherent redundancy/fault tolerance can be readily achieved by adding more than 3 axes of control.

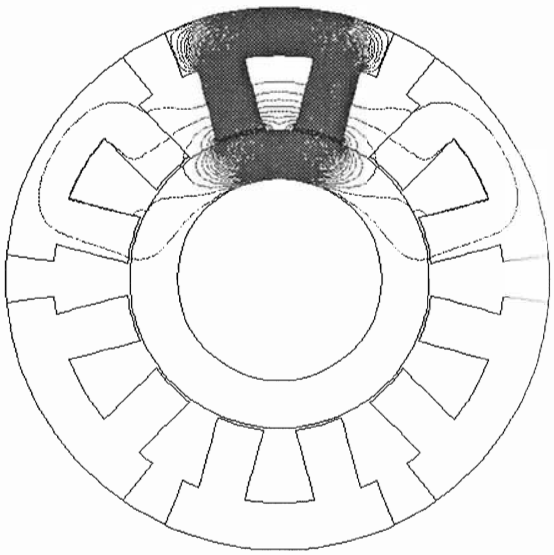

Figure 4: Flux Plot with Single Winding Excitation

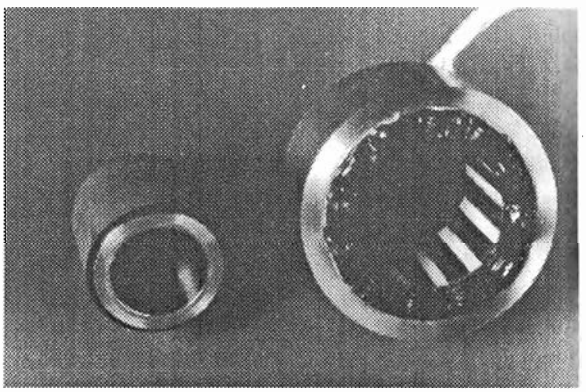

Figure 5: Test Rig Radial Magnetic Bearing

Figure 5 shows the fault-tolerant radial magnetic bearing used in a single-spool test rig described later in this paper. The radial bearing is sized to generate 500

lbs radial force with 2 active axes. This magnetic structure for the stator can be constructed using a stack of composite laminations as has been done for electric machine rotors or by bonding solid non-magnetic segments to a stack of laminations as has also been done for electric machine rotors (Kliman, 1987) (Kliman, 1989). The bearing laminations are made from a Cobalt-Iron alloy which has superior magnetic, thermal degradation and mechanical properties.

The test rig axial active magnetic bearings (Figure 6) are configured in a similar fashion with 2 magnetically independent control axes, each control axis with 100% force capability (1000 lbs) - thus 1 of the 2 available control axes are required for rated thrust loading. An alternative axial bearing configuration planned for larger thrust loads would have a 3 disk structure each with 50% axial force capability (2 of 3 required).

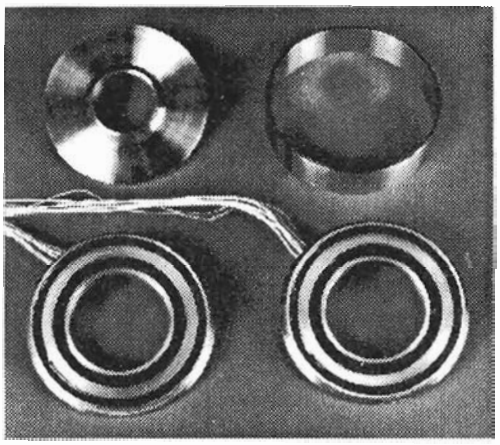

Figure 6: Test Rig Axial Magnetic Bearing

MAGNETIC BEARING CONTROLS

Figure 7 illustrates a proposed fault-tolerant AMB control system. The controls consist of 2 hierarchical levels: a supervisory level (BSC - bearing system controller) and an actuation level (AXC - axis controller). The supervisor controllers are configured in a duplex fault-tolerant configuration, with one supervisor in active control and the second in an active standby mode. Each bearing system controller is configured to control one engine rotor, including as envisioned here: 3 axis controllers for rb1, 3 axis controllers for rb2, and 3 axis controllers for the axial bearing. A typical twin spool aircraft engine will require 2 such systems.

Communication between the supervisory and actuation levels is accomplished in a manner to maintain electrical isolation e.g. fiberoptic communication links. Each axis controller is capable of accepting 2 command streams from each of the duplex bearing system controllers via high-bandwidth half-duplex serial communication channels.

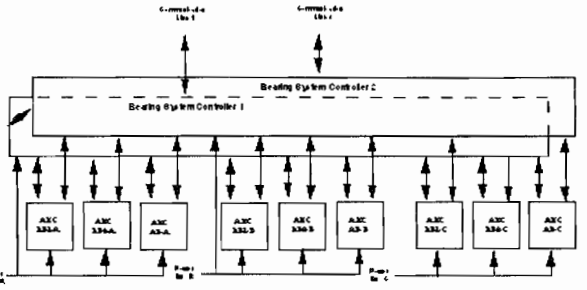

Figure 7: Single Spool Active Magnetic Bearing Control System with Duplex Supervisor

The bearing system controller is responsible for control of the coupled bearings, along with rotor position and active vibration control. Each of the axis controllers linearizes its unbiased magnetic actuator and functions as an inner force control loop. Each axis controller accepts a force command from the bearing system controller and supplies feedback estimates of gap length and velocity along its axis. The axis controller regulates rotor flux and uses a reluctance model of the electromagnetic actuator to calculate the stator flux linkage required to provide the commanded force.

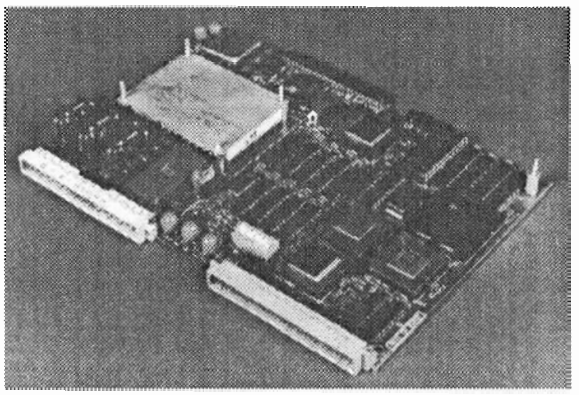

Figure 8: Single Board Axis Controller

The actuation controllers are essentially smart, self-protecting, power amplifiers capable of exciting a single independent AMB axis (2 electromagnetic windings, + and -). Figure 8 shows an axis controller developed to supply 50A maximum at 270V. The AXC board is a VMEbus slave module based on a 320C31 DSP containing a hybrid IGBT power module and all the requisite interface and protection circuits. An air cooled heatsink attaches to the top board surface to create a self contained double-width VME module.

The prototype AMB control system developed for control of the laboratory test rig is shown in Figure 9. The VME based control system contains 8 axis controller modules and a single bearing system

controller which is a 320C30 DSP based VMEbus master. The prototype system uses shared memory and the VME backplane for intermodule communication in lieu of serial communications links. This prototype control system contains a full complement of axis controllers but currently has no redundancy at the bearing system controller level and is subject to single point failures along the VME backplane. A redundant 320C40 DSP based supervisor is being implemented.

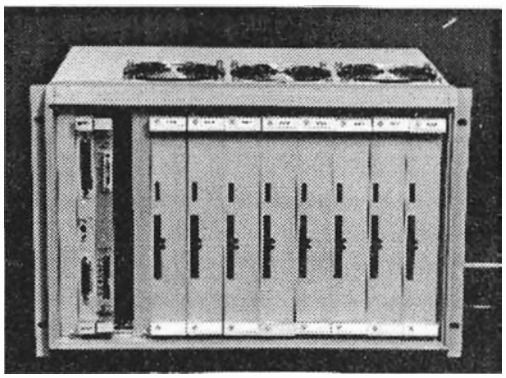

Figure 9: AMB Control Rack

Force Transformations

The actuation commands produced by the AMB control algorithms are desired orthogonal forces f_y and f_z for each radial bearing along with desired axial force f_x. The desired radial forces must be produced by f_a, f_b, f_c forces in line with the three actuator axes available at each radial bearing. The force vector f_{yz} (with 2 elements along the *yz* axes) can be related to the developed force vector f_{abc} by the transformation matrix B as follows:

$$f_{yz} = B * f_{abc} \ , \text{ where } B = \begin{bmatrix} \sin\frac{\pi}{3} & \sin 0 & \sin\frac{5\pi}{3} \\ \cos\frac{\pi}{3} & \cos 0 & \cos\frac{5\pi}{3} \end{bmatrix}.$$

When all three axes are available, a redundant force actuator exists, and the forces will be distributed to the three axes in order to produce the desired force vector with the minimum possible forces in all three axes. This distribution is the least squares solution $(\min\|f_{abc}\|_2 = \min(f_a^2 + f_b^2 + f_c^2)^{\frac{1}{2}})$ to the above set of underdetermined linear equations given as:

$$f_{abc} = B^+ f_{yz}, \text{ where } B^+ = B^T(BB^T)^{-1} = \begin{bmatrix} \frac{1}{\sqrt{3}} & \frac{1}{3} \\ 0 & \frac{2}{3} \\ \frac{-1}{\sqrt{3}} & \frac{1}{3} \end{bmatrix}$$

represents the pseudo-inverse of the original transformation matrix B.

This force distribution is not unique and alternate distribution strategies are possible. One alternative produces a reference force vector f_{abc} which minimizes the rms currents commanded in the electromagnetic actuators and associated losses. Since actuator force is proportional to i^2 this strategy corresponds to choosing the unique f_{abc} with minimum 1-norm $(\min\|f_{abc}\|_1 = \min(|f_a|+|f_b|+|f_c|))$. This strategy does not, however, fully utilize the force capability of the actuator.

When one axis is unavailable, the two remaining actuators can still maintain full control by producing a radial force vector of arbitrary direction and degraded maximum amplitude. The transformation between the orthogonal and coupled reference frames under these circumstances is deterministic. The resultant relationships with axis *c* failed are:

$$f_{yz} = B_{ab} * f_{ab} \ , \ B_{ab} = \begin{bmatrix} \frac{\sqrt{3}}{2} & 0 \\ \frac{1}{2} & 1 \end{bmatrix} \text{ then}$$

$$f_{ab} = B_{ab}^{-1} * f_{yz} \ , \ B_{ab}^{-1} = \begin{bmatrix} \frac{2}{\sqrt{3}} & -\frac{1}{\sqrt{3}} \\ 0 & 1 \end{bmatrix}.$$

The relationships with axes *a* and *b* failed respectively follow in a similar fashion.

Measurement Transformations

Feedback information corresponding to gap lengths and velocities is measured by axis controllers operating in an *abc* reference frame. These measurements must be transformed into the *yz* reference frame in order to close the feedback loops within the centralized radial bearing control. Measurements in these two frames can be related by :

$$l_{abc} = A * l_{yz} \text{ where } A = \begin{bmatrix} \sin\frac{\pi}{3} & \cos\frac{\pi}{3} \\ \sin 0 & \cos 0 \\ \sin\frac{5\pi}{3} & \cos\frac{5\pi}{3} \end{bmatrix}.$$

When all three axes are active and measuring their respective air-gap lengths, a redundant sensor exists and the desired transformation should average the 3 available measurements to obtain the required 2 *yz* equivalents. This represents the least squares solution to an overdetermined linear system (i.e. min $\|l_{abc} - A\, l_{yz}\|_2$) given by

$$l_{yz} = A^+ l_{abc} \text{ where } A^+ = (A^TA)^{-1}A^T = \begin{bmatrix} \frac{1}{\sqrt{3}} & 0 & \frac{-1}{\sqrt{3}} \\ \frac{1}{3} & \frac{2}{3} & \frac{1}{3} \end{bmatrix}.$$

When one axis is unavailable, the two remaining axes are sufficient to locate the rotor position relative to the magnetic bearing stator. The transformation between the orthogonal and coupled reference frames under these circumstances is deterministic. The resultant relationships with axis *c* failed are:

$$l_{ab} = A_{ab} * l_{yz}, \text{ where } A_{ab} = \begin{bmatrix} \frac{\sqrt{3}}{2} & \frac{1}{2} \\ 0 & 1 \end{bmatrix} \text{ consequently}$$

$$l_{yz} = A_{ab}^{-1} * l_{ab}, \quad A_{ab}^{-1} = \begin{bmatrix} \frac{2}{\sqrt{3}} & -\frac{1}{\sqrt{3}} \\ 0 & 1 \end{bmatrix}.$$

The relationships with axes *a* and *b* failed respectively follow in a similar fashion.

Assuming that the noise inherent in the three gap measurements is gaussian with zero mean and a standard deviation σ, we can estimate the rms noise in the *yz* measurements. Using the fact that variance of sum of measurements is the sum of variances, when all three measurements are available, $l_{yz} = A^{+} l_{abc}$ and the rms value of noise is then given by

$$\sigma_y = \left(\left(\frac{1}{\sqrt{3}} \right)^2 + \left(\frac{-1}{\sqrt{3}} \right)^2 \right)^{\frac{1}{2}} \sigma = \sqrt{\frac{2}{3}}\sigma \ ,$$

$$\sigma_z = \left(\left(\frac{1}{3} \right)^2 + \left(\frac{2}{3} \right)^2 + \left(\frac{1}{3} \right)^2 \right)^{\frac{1}{2}} \sigma = \sqrt{\frac{2}{3}}\sigma \ .$$

When the measurement along axis c is failed the relation is $l_{yz} = A_{ab}^{-1} * l_{ab}$ and the rms noise is given by

$$\sigma_y = \left(\left(\frac{2}{\sqrt{3}} \right)^2 + \left(\frac{-1}{\sqrt{3}} \right)^2 \right)^{\frac{1}{2}} \sigma = \sqrt{\frac{5}{3}}\sigma \ , \quad \sigma_z = \sigma.$$

For example, when *c* measurement fails, note that the noise in the *y* measurement increases by a factor of $1.6 \left(\sqrt{\frac{5}{3}} \div \sqrt{\frac{2}{3}} \right)$, while the noise in the *z* measurement increases by a factor of 1.22.

MAGNETIC BEARING TEST RIG

The test rig shown in Figure 10 was developed for validation testing of advanced magnetic bearings and controls. The test rig utilizes two control radial magnetic bearings located fore and aft, a disturbance radial magnetic bearing located at approximately mid-span, a control thrust magnetic bearing, and a disturbance thrust magnetic bearing. The forward direction is to the left. Radial auxiliary bearings are mounted out-board of the radial magnetic bearings. The radial auxiliary bearings are turbine engine class bearings, and the radial clearance between the shaft OD and the bearing inner ring ID is equal to 0.0254 cm (10 mils) while the radial clearance of the magnetic bearings is equal to 0.0508 cm (20 mils). An axial auxiliary or bumper bearing is utilized to prevent damage to the thrust magnetic bearing.

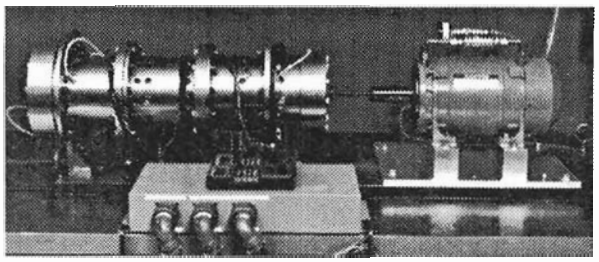

Figure 10: High Speed Magnetic Bearing Test Rig

Overhung disks, fore and aft, simulate a fan and turbine and provide balance planes for mechanical balancing. The rig is driven by a 20 HP electric motor through a quill drive shaft located at the aft end of the rotor.

EXPERIMENTAL RESULTS

Fault tolerance testing was conducted on the test rig while rotating it at 3000 rpm. First, *a*, *b*, and *c* force actuators were failed one at a time. The *y* and *z* measurements are plotted in Figure 11 along with the radial measurement (ρ). The other variable shown is a fault status indicating first *a* actuator failure, followed by *b* actuator failure, then *c* actuator failure. As can be seen during each individual actuator failure the remaining two actuators successfully take up the force production with no appreciable change in gap lengths or noise on the gap measurements.

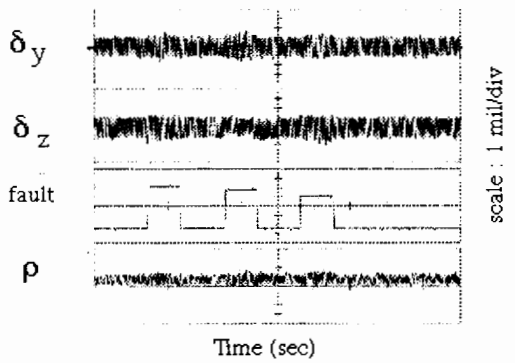

Figure 11: Actuator Failure

Table 1 reports the experimental results when the

measurements along *a*, *b*, and *c* are failed one at a time. The predicted changes in rms value of the measurement noise are tabulated below with the corresponding measurements from the test rig. The predictions are in close agreement with the measurements.

Axis Failed	% increase along y Measured	% increase along y Predicted	% increase along z Measured	% increase along z Predicted
A	70	60	27	22
B	20	0	60	70
C	60	60	47	22

Table 1: RMS noise with measurement failure

Figure 12 plots the results when both the measurements and actuators along *a* , *b* and *c* axes are sequentially failed. We see that the fault-tolerant bearing system indeed performs well, although with increased noise when measurements fail, as predicted.

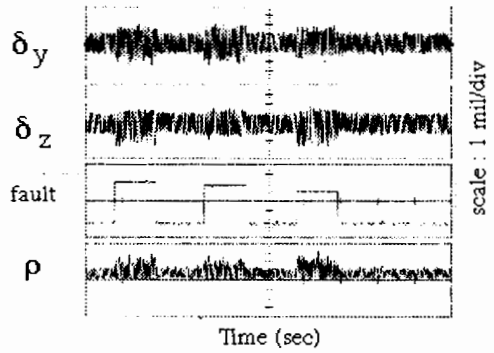

Figure 12: Actuator and Measurement Failure

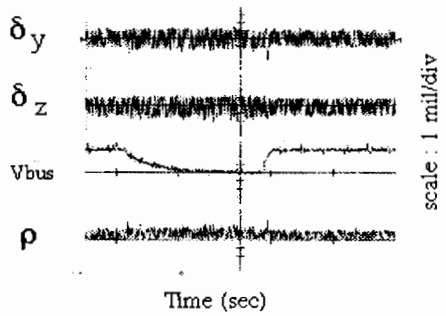

Figure 13: Bus Failure with measurement not failed

Tests were then conducted with the controller successfully maintaining rotor suspension when one complete electrical bus is failed, disabling both force actuators RB1-C and RB2-A. Figure 13 shows little effect from this bus failure. Figure 14 repeats this bus failure test with the measurements along these axes also failing. The result is a somewhat larger transient disturbance and more signal noise as predicted by the failed measurement.

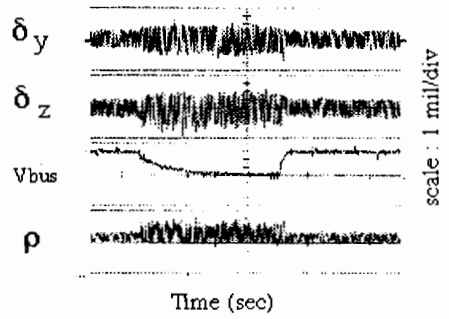

Figure 14: Bus Failure with measurement failure

CONCLUSIONS

This paper has presented a fault-tolerant active magnetic bearing system which has been shown capable of controlled rotor suspension during and after actuator, controller, and measurement faults.

Further development of the active magnetic bearing system for aircraft engine applications will pursue size and weight reduction of fault-tolerant controls, a "sensorless" feedback scheme whereby the actuator windings double as position sensors, and integration of a hydrostatic gas backup bearing along with self lubricated touchdown bearing into the fault-tolerant magnetic structures.

REFERENCES

1. Kliman, G.B., 1987, "Composite Rotor Lamination for Use In Reluctance, Homopolar and Permanent Magnet Machines," U.S. Patent No. 4,916,346.
2. Kliman, G.B., 1989, "Method of Fabricating Composite Rotor Laminations for Use In Reluctance, Homopolar and Permanent Magnet Machines," U.S. Patent No. 4,918,831.
3. Yates, S.W. and Williams, R.D., "A Fault-Tolerant Multiprocessor Controller for Magnetic Bearings," IEEE Micro Magazine, August 1988, pp. 6-17.
4. Gondhalekar, V. and Holmes, R., "Design of a Radial Electromagnetic Bearing for the Vibration Control of a Supercritical Shaft," Procedures of the Institute of Mechanical Engineers, Vol. 198C No. 16, pp. 235-242.